Journal of Hazardous Materials 178 (2010) 171–179

Contents lists available at ScienceDirect

Journal of Hazardous Materials

journal homepage: www.elsevier.com/locate/jhazmat

The application of zero-valent iron nanoparticles for the remediation of a uranium-contaminated waste effluent

Michelle Dickinson*, Thomas B. Scott

Interface Analysis Centre, 121 St. Michael's Hill, University of Bristol, UK

ARTICLE INFO

Article history:
Received 20 October 2009
Received in revised form 11 January 2010
Accepted 13 January 2010
Available online 20 January 2010

Keywords:
Iron
Nanoparticles
Uranium
Remediation
Zero-valent

ABSTRACT

Zero-valent iron nanoparticles (INP) were investigated as a remediation strategy for a uranium-contaminated waste effluent from AWE, Aldermaston. Nanoparticles were introduced to the effluent, under both oxic and anoxic conditions, and allowed to react for a 28-d period during which the liquid and nanoparticle solids were periodically sampled.

Analysis of the solution indicated that under both conditions U was removed to <1.5% of its initial concentration within 1 h of introduction and remained at similar concentrations until approximately 48 h. A rapid release of Fe into solution was also recorded during this initial period; attributed to the limited partial dissolution of the INP. XPS analyses of the reacted nanoparticulate solids between 1 and 48 h showed an increased Fe(III):Fe(II) ratio, consistent with the detection of iron oxidation products (akaganeite and magnetite) by XRD and FIB. XPS analysis also recorded uranium on the recovered particulates indicating the chemical reduction of U(VI) to U(IV) within 1 h. Following the initial retention period U-dissolution of U was recorded from 48 h, and attributed to reoxidation.

The efficient uptake and retention of U on the INP for periods up to 48 h provide proof that INP may be effectively used for the remediation of complex U-contaminated effluents.

1. Introduction

In recent years, iron nanoparticles (INP), amongst other metallic nanoparticles, have received much attention for their potential application to the treatment of contaminated soils and waters. Their high surface area to volume ratio and high surface energy [1] means that INP offer a greater reactivity than the surfaces of bulk scrap metal or iron filings/granules commonly used for remediation purposes in permeable reactive barriers, injection, etc., see Tratynek [2] and Bigg and Judd [3] for reviews. The remediation mechanism depends on the nature of the contaminant but in all cases is driven by the oxidation of Fe(0) [4]. In the case of chlorinated organics, the harmful target contaminant is reductively transformed to relatively innocuous species, whilst for waters containing heavy metals, decontamination occurs via sorption and/or reduction onto the surface of the iron. It has repeatedly been demonstrated that INP degrade contaminants more rapidly than the aforementioned forms of zero-valent iron [5–12].

To date, iron nanoparticles have been shown to be effective remediators of a range of contaminants including chlorinated organics [1,5–7,11,13–16] and inorganic anions [8,17–20] amongst others [4,15,21–23]. In addition, INP have also been shown to successfully remediate solutions contaminated with a range of metals, including Pb [10,12,24], Cr [4,10,17,21,24], Cu [4,12,21], As [20,25,26], Ni [12], Zn [12], Cd [12] and Ag [12]. The application of zero-valent INP for the remediation of radionuclides remains less widely researched than for the aforementioned heavy metals and organic contaminants. Studies are limited to the radioisotopes of Ba [27] and TcO_4 [24,28], and our group's U-sorption investigations [29,30]. It has long been known that scrap/bulk iron and iron-based minerals are highly effective scavengers of the uranium radionuclide [31,32]. Removal of uranium from solution is attributed to the adsorption of uranyl ions (UO_2) onto iron corrosion products [33,34] and the reductive precipitation of soluble U(VI) into the less soluble U(IV) [35–39].

To date, views are mixed regarding the actual mechanism for the removal of soluble U by zero-valent iron. As Fe(0) is a stronger reducing agent than Fe(II), it was previously thought that contaminant reduction was driven by the oxidation of Fe(0) to Fe(II) [40]. However, White and Peterson's [41] study determined the oxidation potential of adsorbed (structural) Fe(II) to be in the range −0.65 to 0.34 V making it a stronger reducing agent than aqueous Fe(II) at −0.77 V, implying that Fe(II)/Fe(III) oxidation may be a significant reaction affecting contaminant reduction. A number of separate studies have shown the reduction of U(VI) to U(IV) by

* Corresponding author. Tel.: +44 0 117 3311171; fax: +44 0 117 9255646.
E-mail addresses: M.Dickinson@bristol.ac.uk, M.Dickinson@googlemail.com (M. Dickinson), T.B.Scott@bristol.ac.uk (T.B. Scott).

0304-3894/$ – see front matter © 2010 Elsevier B.V. All rights reserved.
doi:10.1016/j.jhazmat.2010.01.060

structural (solid) Fe(II) [29,33,36,37,42–45]. This theory was corroborated by Charlet et al. [36] who found that the final oxidation reduction potential (ORP) following the Fe-driven reduction of uranium corresponded to the Fe(II)/Fe(III) couple rather than that of Fe(0)/Fe(II).

In previous laboratory studies [29,30], INP have shown high affinity for U-uptake, with the maximum U-removal of ~99% occurring from 1000 ppm U-solutions within the first 4 h of exposure, for solutions with pH 5–pH 6 [29]. Results also indicate that the reaction mechanism for U-uptake may vary at different solution pHs [30]. At mildly acidic pH, U-removal occured via two reaction mechanisms; the precipitation of $UO_3{\cdot}2H_2O$ (metashoepite) onto the surface and the reductive precipitation of UO_2. Metashoepite precipitation was not observed to occur at basic-neutral pH. Reductive precipitation of the U(VI) adsorbed onto the surfaces of the INP was also observed to occur most rapidly at basic pH.

The current work presents a case study of the application of INP to a contaminated waste effluent from the Atomic Weapons Establishment (AWE), Aldermaston site in the UK. The effluent originated from research processes and was predominantly liquid with a minor sediment/sludge component (<1%). A significant proportion of the total uranium concentration was determined to exist within the sediment phase and so could be readily removed via settlement and separation of this material. However, low concentrations of aqueous ^{238}U remain were determined in the liquid, and it was this contaminant component that was targeted for removal using INP. The liquid effluent contained a range of other chemical components including chloride, sulphate, phosphate and nitrate, in addition to low (<1.5 ppm) concentrations of Sr, Zn, Al, Pb, Ni, Cu and Cr. The concentrations of the aforementioned components are all below the permissible release limits for water entering the local drainage systems [46] and, as such, are not targets for remediation. However, the complex chemical makeup of the effluent provides a useful test of the nanoparticles' ability to remediate U from 'real' systems, having proven their efficacy in otherwise simple systems where there are no competing reactions. It is known that INP are able to reduce nitrates [4,8,17,47,48] and it has also been reported that in the presence of competing ions such as HCO_3^-, SiO_4^{2-} and PO_4^{3-} the efficacy of As(V) adsorption onto INP was reduced [25].

The aim of this study was to investigate the ability of INP to remediate a particular U-contaminated effluent. Factors investigated include the uptake efficiency and duration of contaminant retention. Nanoparticles were added to the effluents, under both oxic and anoxic conditions and left to react for a minimum period of 28 days. Aliquots of solid/liquid suspensions were taken at various intervals and a multi-disciplinary approach was adopted to further elucidate the uptake mechanisms of U onto the INP. Inductively coupled plasma-atomic emission spectroscopy (ICP-AES) and inductively coupled plasma-mass spectrometry (ICP-MS) were used to study the Fe- and U-concentrations, respectively, in solution. The nanoparticulate solids were also analysed by a variety of techniques: X-ray diffraction (XRD) was used to study the changes to the bulk material; focussed ion beam (FIB) imaging was used to examine their surface morphology and microtexture; scanning electron microscopy-energy dispersive X-ray analysis (SEM-EDX) was used to confirm the elemental composition of corrosion products and X-ray photoelectron spectroscopy (XPS) analysis was performed to study the surface chemistry of the INP and any sorbed species.

2. Materials and methods

2.1. Chemicals

All chemicals (iron sulphate ($FeSO_4{\cdot}7H_2O$), sodium hydroxide (NaOH), sodium borohydride ($NaBH_4$), nitric acid (HNO_3)), and solvents (ethanol, acetone) used in this study were of analytical grade and all solutions were prepared using Milli-Q purified water (resistivity > 18.2 MΩ cm). The glovebox used to perform the anoxic experiments was filled with oxygen-free N_2 gas from BOC.

2.2. Nanoparticle synthesis

The iron nanoparticles were synthesised following an adaptation of the method first described by Wang and Zhang [5], using sodium borohydride to reduce ferric iron to a metallic state via the following reaction:

$$4Fe^{3+} + 3BH_4^- + 9H_2O \rightarrow 4Fe(0)\downarrow + 3H_2BO_3^- + 12H^+ + 6H_2 \quad (1)$$

Briefly, 7.65 g of $FeSO_4{\cdot}7H_2O$ was dissolved in 50 ml of Milli-Q water (18.2 MΩ cm) and then a 4 M NaOH solution was used to adjust the pH to the range 6.2–7. The salts were reduced to metallic nanoparticles by the addition of 3.0 g of $NaBH_4$. The nanoparticle product was isolated through centrifugation and then sequentially washed with water, ethanol and acetone (20 ml of each). The nanoparticles were dried in a dessicator under low vacuum (approx 10^{-2} mbar) for 48 h and then stored in the oxygen-free nitrogen environment of a Saffron Scientific glovebox until required.

2.3. Experimental methodology

Experiments were performed under anoxic conditions, to study the mechanisms of removal, and in the open laboratory (oxic), to be more representative of treatment systems likely to be implemented. In one anoxic batch the U-concentration was artificially elevated to be more readily detectable in XPS. A control system comprising the effluent with no INP was also studied to investigate whether U-sorption to the reaction vessel occurred. The four different experimental systems are summarised in Table 1.

400 ml of effluent was decanted into each of four 500 ml borosilcate/glass jars. Prior to introducing the INP to the anoxic systems, the effluents were purged of any dissolved oxygen by bubbling nitrogen gas through them within the oxygen-free environment of a nitrogen-filled Saffron Scientific glovebox and then allowing the liquid to stabilise/acclimatise for 24 h. Dissolved oxygen levels in each system were measured using a Jenway Model 970 Dissolved Oxygen meter prior to the addition of the INP. Effluent system B was spiked with 2 ml of 1000 ppm U in nitric acid and the pH readjusted to near-neutral conditions using 4 M NaOH to compensate for the shift to acidic conditions.

To each system, 0.05 g of nanoparticles suspended in 2.5 ml of ethanol (dispersed by sonicating for 10 min) were added. Each system was studied at 1 h, 2 h, 4 h, 12 h, 24 h, 48 h, 7 d, 14 d and 28 d. Prior to sampling, the jars were gently shaken to ensure homogeneity and then aliquots of 10 ml were taken. The suspensions were centrifuged to separate the liquid and solid phases and the liquid was decanted into a beaker. Approximately half of the liquid was taken for pH and ORP measurements, using a Hanna Instruments meter (model HI 8424) with a combination gel electrode pH probe and a platinum ORP electrode (model HI 3230B), respectively. The remaining liquid was filtered through a 0.22 μm cellulose acetate filter into a 15 ml centrifuge tube and a drop of concentrated HNO_3 was added to prevent sorption to the vessel walls prior to further preparation for ICP-AES and ICP-MS analysis. At the sampling periods 1 h, 4 h, 24 h, 48 h, 7 d, 14 d and 28 d the solids remaining after decantation were prepared for analysis by sequential rinsing in 3 ml each of Milli-Q water, ethanol and then acetone. At some of these sampling periods, the water rinse from systems B and C was also prepared for analysis in order to study the physisorbed species. Solid samples were prepared by pipetting a small volume of material onto the appropriate stubs/glass slides for XPS, FIB and

Table 1
A summary of the four effluent systems studied.

System	Conditions	Solution	Treatment	Experiment
A	Anoxic	Effluent, as delivered	INP	Anoxic sorption
B	Anoxic	Effluent with increased U (~2.5 ppm)	INP	Mechanistic studies
C	Oxic	Effluent, as delivered	INP	Oxic sorption
D	Oxic	Effluent, as delivered	None	Sorption control

XRD and allowing them to dry under low vacuum or within the nitrogen-filled glovebox.

2.4. ICP-AES preparation

The liquid samples were prepared for ICP-AES analysis by a 10 times dilution in 1% nitric acid (analytical quality concentrated HNO_3 in Milli-Q water). Blanks and standards for analysis were also prepared in 1% nitric acid, with Fe standards of 0.1, 0.25, 0.5, 1, 2.5, 5 and 10 ppm. A Jobin Yvon Ultima ICP-AES (sequential spectrometer) fitted with a cyclone spray chamber and a Burgener Teflon Mira Mist Nebulizer was used. The Fe-concentration was measured using the emission line at 259.94 nm.

2.5. ICP-MS preparation

Samples from systems A, C and D were prepared for ICP-MS analysis by a 10 times dilution (most samples) in 1% nitric acid (analytical quality concentrated HNO_3 in Milli-Q water). Samples from system B, with elevated U-concentrations, were diluted by a factor of 10,000. Blanks and uranium standards at 0.1, 0.5, 1, 5 and 10 ppb were also prepared in 1% nitric acid. An internal Bi standard of 10 ppb was added to blanks, standards and samples. The ICP-MS instrument used was a Thermo Elemental PQ3.

2.6. FIB

A FEI FIB Strata 201 was used to examine the sample morphology and microtexture of the nanoparticulate solids. The resolution of the system is dependent on the operating conditions of the system, for example, at 30 kV, the resolution is 500 nm for an operating current above 11 nA and at least 5–7 nm for a current of 1 pA.

2.7. XPS

Solid samples were analysed at $<5 \times 10^{-8}$ mbar in a Thermo Fisher Scientific Escascope equipped with a dual anode X-ray source ($Al_{K\alpha}$ 1486.6 eV and $Mg_{K\alpha}$ 1253.6 eV). $Al_{K\alpha}$ radiation was used at 400 W (15 kV, 23 mA). High resolution scans were acquired using a 30 eV pass energy and 200 ms dwell times. Following the acquisition of 'wide' spectra over a wide binding energy range, the regions containing the Fe, Ni, C, O and U peaks were scanned at a higher energy resolution. Data analysis was carried out using Pisces software [49] with binding energy values of the recorded lines referenced to the adventitious hydrocarbon C1s peak at 284.8 eV.

2.8. XRD

A Phillips Xpert Pro diffractometer with a $Cu_{K\alpha}$ radiation source ($\lambda = 1.5406$ Å) was used for XRD analysis (generator voltage of 40 keV; tube current of 30 mA). XRD spectra were acquired between 2θ of 0–90°, with a step size of 0.02° and a 2 s dwell time.

2.9. SEM-EDX

EDX analysis was performed using a permanent thin film window Link (Oxford Instruments) detector and WinEDS software in a Hitachi S2300 SEM using an electron beam operating voltage of 25 kV and emission current of 60–70 μA.

3. Results and discussion

3.1. Initial conditions of the AWE effluent

Prior to addition of the INP, the pH, ORP and dissolved oxygen (DO) of each system was measured; initial conditions are summarised in Table 2. The concentration of uranium was found to vary between batches of effluent, with the lowest concentration measured in system C. This may be attributed to slight differences between batches of effluent received from AWE and the complex relationship between the pH and U-solubility. The solubility of U is lowest at around pH 7, as demonstrated by Noubactep [50]. It was decided not to alter the effluent from the "as delivered" state, with the exception of system B.

3.2. Initial characterisation of nanoparticles

Prior to the addition of the Fe nanoparticles to the effluent solutions, FIB imaging showed individual particles to be roughly spherical and loosely aggregated into chains when dried, a feature attributed to their magnetic cores [51]. XRD analysis indicated the presence of poorly crystalline/amorphous metallic iron. XPS data confirmed the presence of metallic iron as well as a magnetite (Fe_3O_4) surface oxide layer. Previous TEM studies showed the oxide thickness to be 3–4 nm whilst BET determined the surface area to be 19.0 m^2/g for nanoparticle manufactured under the same conditions [52].

3.3. Solution analysis

The pH, ORP, U- and Fe-concentrations were measured at different reaction times for each system. Analysis of the effluent solution from a control system containing no nanoparticles showed a steady U-concentration, providing evidence that the U did not simply sorb to the reaction vessels.

From the systems containing INP the reactions appeared to progress through three stages, roughly split into the periods 0–48 h, 48 h to 14 d, 14–28 d.

3.4. 0–48 h

Immediately following the addition of the INP to systems A and C (anoxic and oxic, respectively) the pH was observed to decrease by 0.4 pH units, reaching local minima at around 2 h, Fig. 1a. The ORP of each nanoparticle system decreased immediately on addition of the INP; the anoxic system (A) reached a minimum value of

Table 2
The initial conditions of each effluent system.

System	pH	ORP (mV)	DO (mg/L)	U (ppb)
A	7.86	167.3	~3	601
B	8.15	139.9	~2	2480
C	7.25	214.7	~10	54
D	7.49	216.0	~12	605

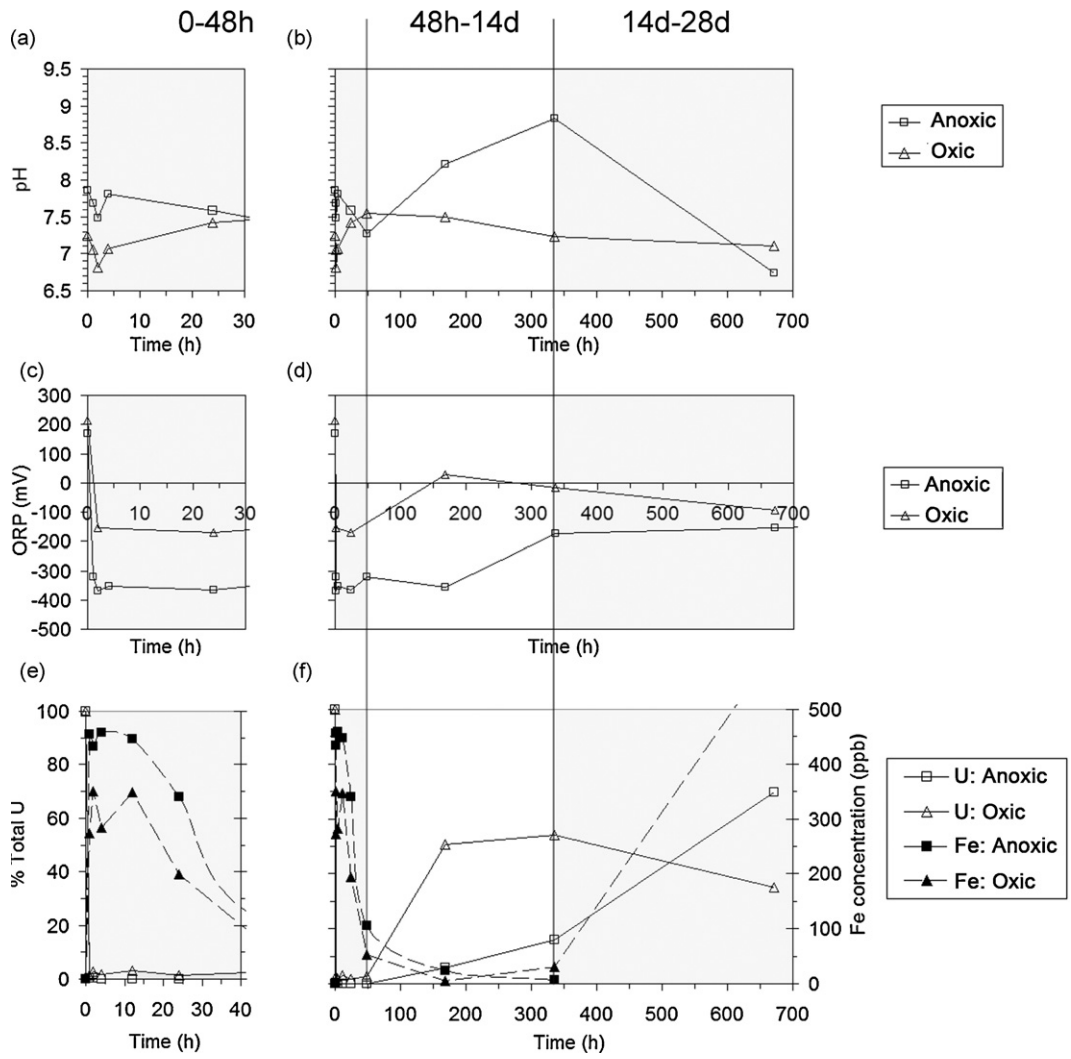

Fig. 1. The pH, ORP, U- and Fe-concentrations in solution at the different sampling periods; (a), (c) and (e) show the reaction time 0–40 h and (b), (d) and (f) show the data acquired over the whole 28-d period, shaded to highlight the three different phases of reaction.

approximately −370 mV at 48 h, and the oxic system (C) reached a minimum of −170 mV slightly earlier at 24 h, Fig. 1c. The immediate reduction in ORP is attributed to rapid consumption of dissolved oxygen and other potential oxidants by the INP. Similarly the slight decrease in pH can be attributed to hydrogen generated from the INP corrosion upon contact with water. Conditions in the oxic system changed more rapidly than the anoxic experiment due to a greater initial quantity of dissolved oxygen, Table 2.

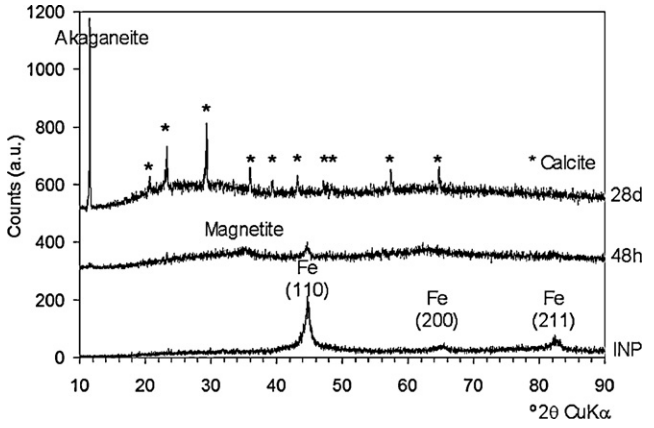

Fig. 2. XRD data acquired from the nanoparticulate solids from system C at 0 h (INP control), 48 h and 28 d.

ICP-MS results recorded a rapid removal of U from solution in systems A and C to 1.5% of the initial concentration and below the detection limit, respectively, within the first hour of the reaction period (Fig. 1e) and remained at, or near, the minimum recorded concentrations until 48 h. The concentration of dissolved Fe in solution increased immediately after the INP addition to all systems, reaching maxima of 284 and 359 ppb in systems A and C, respectively, within the first 4 h. The Fe-concentration in solution remained at, or near, the maximum until 24 h in the anoxic system (A) but only 12 h in the oxic system. This maximum release of iron occurred concurrently with maximum U-uptake and the minimum recorded pH and ORP.

3.5. 48 h to 14 d

Following the decrease to local mimina, the pH of each system then displayed a general upward trend with the oxic and anoxic systems reaching maxima at 48 h and 14 d, respectively. The ORP increased to near-zero levels in the oxic system and −170 mV in the anoxic system. The U-concentration in solution increased during this period whilst Fe-concentration decreased. The results indicate the onset of partial redissolution of uranium previously removed on the INP surfaces.

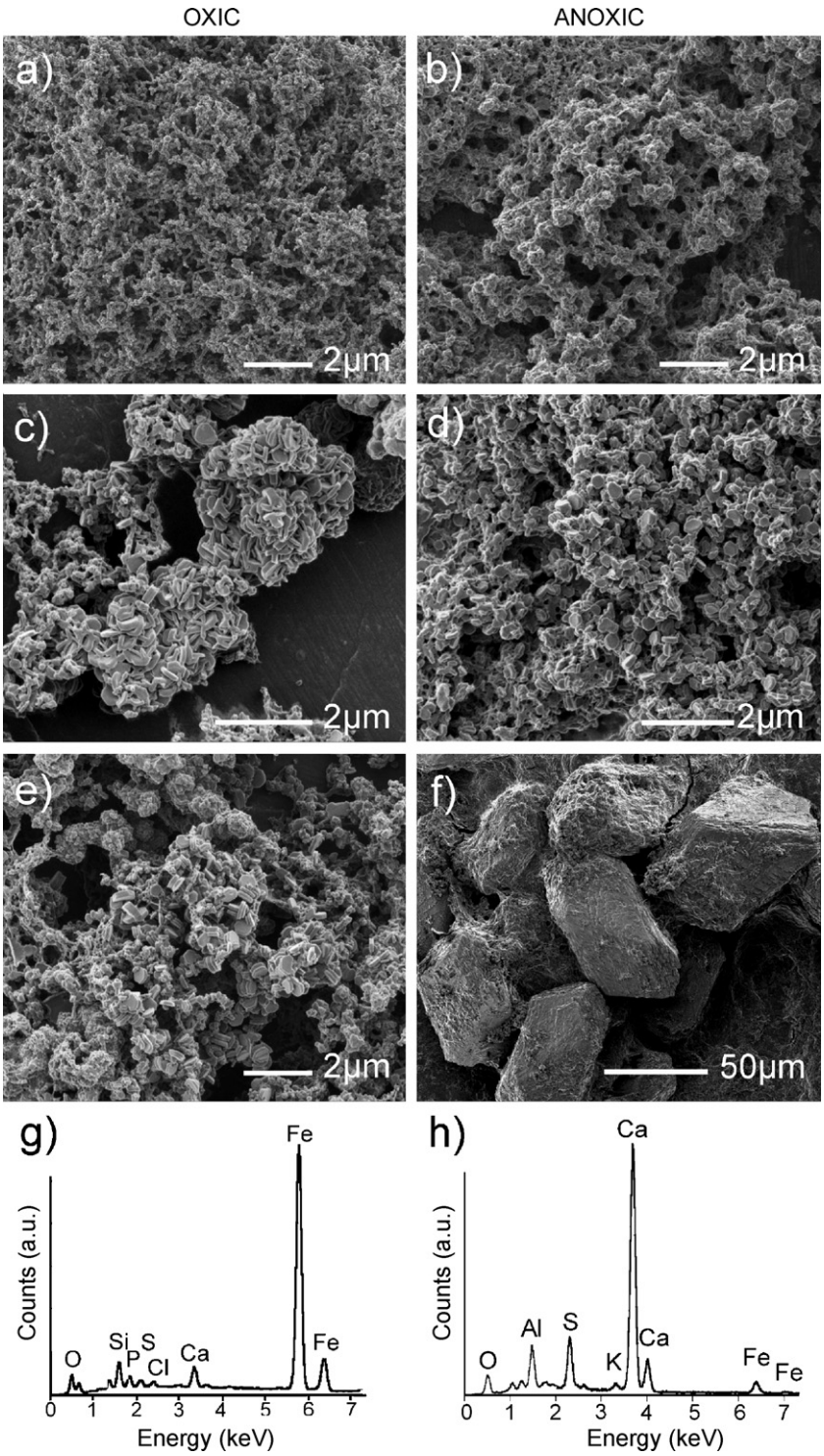

Fig. 3. Focussed ion beam (FIB) induced secondary electron images of the reacted nanoparticle solids and EDX spectra acquired from systems A and C at different sampling periods (a) INP standards (b) system C, 48 h; (c) system A 7 d; (d) system C, 7 d; (e) system A, 14 d; (f) system C, 14 d; (g) EDX spectrum acquired from system A at 48 h; (g) EDX spectrum acquired from system C at 28 d from a region containing calcite crystals.

3.6. 14 d to 28 d

In the anoxic system (A) the U-concentration increased gradually to 15% of the total initial U by the final sampling point (Fig. 1f). In the oxic system, the U-concentration increased more significantly and stabilised at approximately 50% of the total initial U between 7 and 14 d. By the 28-d sampling period the U-concentrations within system A had decreased slightly to 35% of its initial concentration.

Analysis of the Milli-q water that had been used to rinse the INP was at near-zero concentrations until 14 d which implied that most of the U was chemisorbed or precipitated on the nanoparticle surfaces. After 14 d the U-concentration in the rinse solution increased to up to 30% of the total U in the oxic system (data not shown) indicating that an increased proportion of U was retarded on the INP in a physisorbed rather than chemisorbed state in the latter stages of the reaction period. In the anoxic system, only 0.6%

of the total U was present in the rinse indicating retention in a more stable chemisorbed state.

3.7. Analysis of reacted nanoparticulate solids

Analysis of the nanoparticulate solids by FIB, XRD and XPS gave results consistent with the reaction stages previously determined from analysis of the liquids. XRD analysis of the reacted nanoparticulate solids from both the oxic and anoxic systems indicated the presence of metallic iron up to 48 h and the oxidation product akaganeite, FeO(OH), was detected from 7 d onwards, Fig. 2. In the oxic system between 48 h and 7 d a broad peak, with low intensity was detected at approx. 35.7°2θ, indicating the presence of a mixed Fe-oxide corrosion product magnetite. From 14 d onwards the akaganeite peak had shifted slightly by approximately −0.4°2θ, which represents an increase in the lattice parameter. This is most likely caused by a cationic substitution of the larger Ca^{2+} ion (0.212 nm compared to 0.166 nm [53]) into the lattice structure of the iron oxidation product. From 14 d the predominant signal detected on the INP solids from the oxic system was calcite, a phase not formed in the anoxic experiment. No uranium phases were detected in either the oxic or the anoxic systems, even that with elevated U. This implies that any bulk U phases formed were either amorphous or at concentrations too low to be detected by XRD.

FIB imaging of the reacted nanoparticulate solids showed crystal structures consistent with phases detected by XRD. After 24 h in solution the nanoparticles were observed to agglomerate as oxidation of the iron began to occur, although no clear magnetite structures were identified. In the anoxic system at 7 d, angular crystals were detected, attributed to akaganeite twins consistent with its detection in XRD. By 14 d small (~0.5 μm) hexagonal plates were visible, also believed to be akaganeite, and the angular crystals had become agglomerated. Samples remained similar in appearance until 28 d.

In the oxic system at 7 d the small hexagonal akaganeite crystals were also present but the sampled material still contained regions of well-defined nanoparticles. The material sampled at 14 d was clumped into large crystalline platelets with large rhombohedral crystals up to ~20 μm in length, consistent with the first detection of calcite by XRD. By 28 d the crystals had grown in size up to 100 μm.

EDX analysis in a SEM was performed on some of the crystalline materials imaged in the FIB to confirm their composition and thus aid their identification. Fig. 3(g) shows the EDX spectra acquired from a region of hexagonal crystals and shows a large Fe and O signal (Al from stub) confirming that they are Fe oxidation products, rather than hexagonal crystals of calcite. Analysis of the rhombohedral crystals observed in nanoparticulate materials from system C from 14 d shows that they are composed mainly of Ca confirming their identification as calcite. Only small Fe peaks were detected possibly indicating the presence of small quantities of siderite ($FeCO_3$) incorporated into the calcite ($CaCO_3$) crystals.

XPS scans acquired over a large binding energy range indicated the sorption of Ca, N, Cl, P, S and Si onto the INP surfaces as early as 1 h into the reaction periods. From the positions of the photoelectron peaks it was possible to identify the chemical state of the elements; N was present as organic N, P as phosphate, S as sulphate and Si as silicates. The position of the Ca peak was indicative of calcium carbonate, consistent with XRD analysis of the oxic system.

The Fe profiles recorded at the different sampling periods for the (anoxic) System B are displayed in Fig. 4. Data from different acquisitions has been rescaled and stacked for easy comparison. The primary Fe $2p_{3/2}$ photoelectron peak recorded from unreacted nanoparticles was centred at 710.3 eV (±0.3 eV), characteristic of magnetite [45]. Additionally, a shoulder was observed at the low

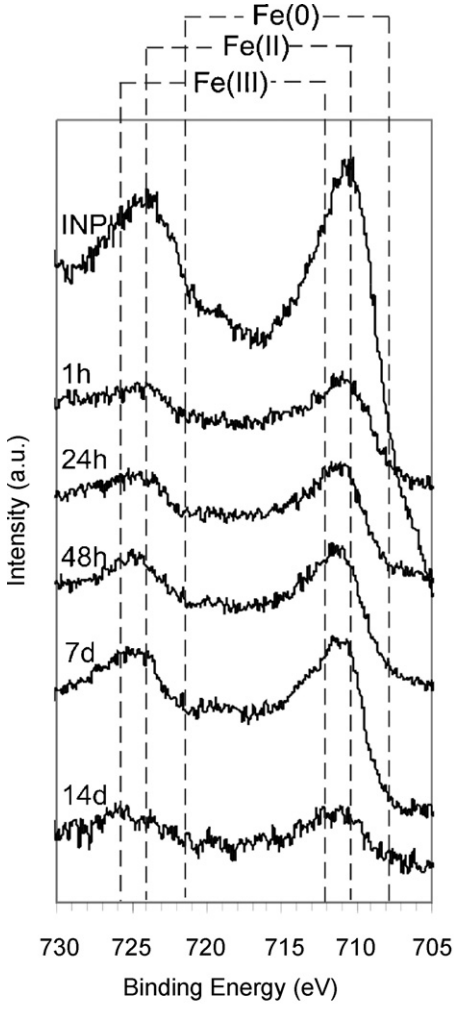

Fig. 4. XPS Fe2p profiles acquired from the reacted nanoparticulate material at progressive reaction times.

energy side, centred at 706.7 eV (±0.3 eV) indicating the presence of metallic iron, Fe(0) [54].

During the reaction period 1–48 h the peaks in the recorded Fe $2p_{3/2}$ profiles displayed a shift to slightly higher binding energies, indicating the oxidation of surfaces. Analysis of the corresponding data acquired from oxic system D showed a more significant shift towards higher binding energies at the 1-h sampling period, indicative of more rapid oxidation than occurred anoxically, probably due to an initial depletion of any DO in solution.

In both systems, curve fitting did not show a clear trend for complete oxidation of magnetite to haematite and the data indicated that magnetite remained the predominant iron oxide species of the nanoparticle surfaces over this period. At 7–14 d in both the anoxic and oxic systems, the peaks in the Fe $2p_{3/2}$ profiles displayed a shift back to a lower binding energy, indicative of the reduction of Fe(III) to Fe(II). This is consistent with the first identification of iron oxidation products in XRD and the FIB and corresponds to the period of maximum Fe-concentration in solution, as Fe(II) is readily dissolved. At later sampling periods the Fe signal became too low to provide any useful information.

The uranium concentration on the surfaces of the INP from the oxic system was too low to be detected even during the period of minimum U in solution. The failure to detect it indicates a heterogeneous distribution and insufficient U to form a complete monolayer. Thus, the U-concentration was artificially elevated in one anoxic system to enable a study of the sorption mechanisms. Curve fittings

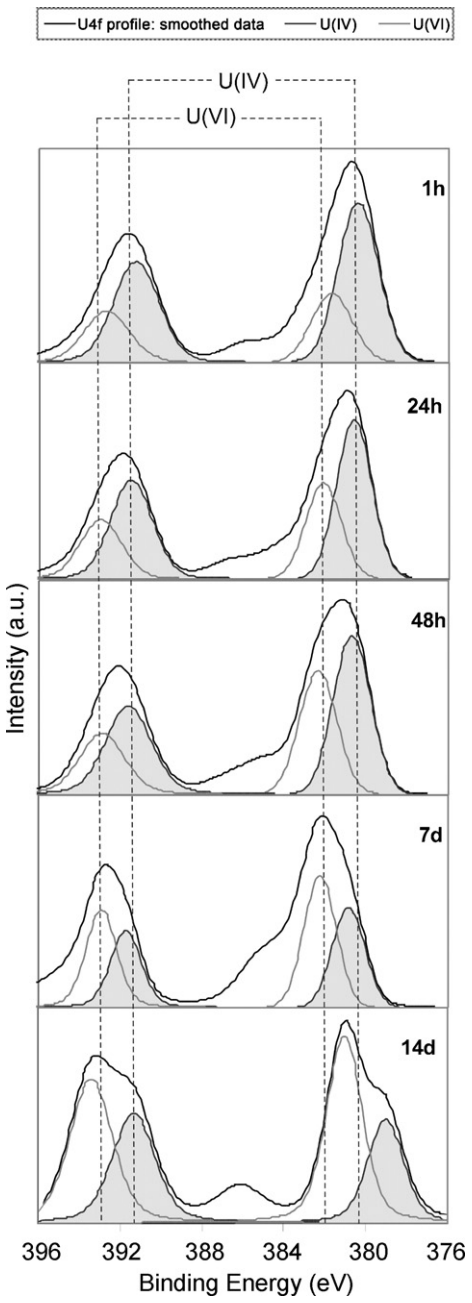

Fig. 5. XPS U4f profiles acquired from the reacted nanoparticulate material highlighted to show the proportion of U(IV) relative to the U(VI) at progressive reaction times. The full scale intensity at subsequent reaction periods are 3000, 3000, 2000, 1100 and 400, respectively.

of the recorded U 4f photoelectron profiles were used to determine the relative proportions of U(VI) and U(IV) in the analysis volume of material. Fig. 5 displays the photoelectron curves for samples taken at 1–14 d periods. The peaks attributed to U(IV) were located at 380.4 eV (±0.3 eV) and 391.5 eV (±0.3 eV), comparing well with values previously reported for non-stoichiometric UO_2, commonly referred to as UO_{2+x}, where $x \leq 2$ [45]. The peaks corresponding to U(VI) are centred at binding energies of 382.2 eV (±0.3 eV) and 392.9 eV (±0.3 eV), and are assigned to UO_3. The profiles are shifted towards the reduced U(IV) peak energies from as early as 1 h into the reaction period, implying rapid reduction concurrent with the oxidation of the iron oxide surface to Fe(II). Curve fitting and analysis showed that U(IV), non-stoichiometric UO_2, accounted for 68% of the U on the surfaces of the nanoparticles at 1 h, decreasing gradually with each sampling period to 34% by the 14-d sampling period, as the U(IV) was gradually reoxidised. The reoxidation of U occurred concurrently with the reduction of Fe(III) to Fe(II), as demonstrated by XPS. The signal intensity of the U 4f photoelectron peak was observed to decrease with time, consistent with the redissolution of U(VI) into solution previously identified from ICP-MS results.

3.8. Summary of reaction mechanisms

The experimental data provides evidence for the removal of U from solution via coupled redox reactions with the INP. The corrosion and sorption mechanisms important for understanding the uptake of metals by INP are described by Eqs. (1)–(5):

Anoxic corrosion:

$$2H_2O + Fe^0 = Fe^{2+} + H_2 + 2OH^- \quad (2)$$

Oxic corrosion:

$$O_2 + 2Fe^0 + 2H_2O = 2Fe^{2+} + 4OH^- \quad (3)$$

and

$$Fe^{2+} + 1/4O_2 + 5/2H_2O = Fe(OH)_3(s) + 2H^+ \quad (4)$$

Cementation:

$$M^{n+} + Fe^0 = M^{n+2} + Fe^{2+} \quad (5)$$

Sorption/ion exchange:

$$> OH + M^{n+} => OM^{n+1} + H^+ \quad (6)$$

where >OH represents an exchangeable ion site [33].

During the first hour of the reaction the immediate removal of U from oxic solution upon addition of the INP is most likely to be described by Eq. (2) and followed (1–4 h) by reaction (3), whereby Fe(0) was oxidised to form a ferrous Fe(II) outer layer. A proportion of this Fe(II) subsequently dissolved into solution, reaching maximum Fe-concentrations over the period where redox conditions were recorded to be most chemically reducing due to the rapid consumption of oxygen (and other potential oxidants) and the production of hydrogen. Meanwhile, U(VI) was removed from solution via sorption (5) with almost immediate reduction to form U(IV). After a period of relative stability the slow ingress of atmospheric oxygen into the reaction system induced the gradual oxidation of Fe(II) to form ferric oxide, Fe(III). At the same time a proportion of the U(IV) was reoxidised to the more soluble U(VI). During the final phase of the experiment, 14–28 d, the redissolved U(VI) was once again removed from solution via sorption onto the surfaces of forming ferrihydrite products (5).

In comparison, the reactions occurring in the anoxic setup would primarily have been driven by anoxic corrosion (1) and the observed removal of U(VI) from solution would be attributed mainly to the cementation process (4).

3.9. Implications for industrial/environmental application

Nanoparticles have previously been investigated as a tool for the remediation of U from simplified systems [29,30] but to date this is the first case study of their application to a real, and complex, effluent arising from industrial processes. The nanoparticles were shown to be effective for the removal of U from these particular solutions, despite any competing mechanisms which may have occurred. No attempts were made to control other parameters such as CO_2, nitrates, sulphates, etc., and U-uptake did not appear to be adversely affected by the presence of the other chemicals. Although relatively low concentrations of U were present in this case study,

it has previously been demonstrated that the INP have the capacity of U-sorption of far higher concentrations [29,30].

This investigation bears direct relevance to the industrial application of INP; the optimum treatment period is 1–48 h after which the iron corrosion process caused the U-redissolution due to a coupled redox reaction with Fe. A continued subject of research is the effect of annealing the INP to determine whether this inhibits, or slows down, the rate of Fe corrosion, and thereby the U-redissolution [52].

4. Conclusions

Zero-valent iron nanoparticles (INP) have been shown to be effective and efficient remediators of a uranium-containing waste effluent from the AWE, Aldermaston site. Uranium was removed from solution to below 1.5% of its initial concentration within the first hour of the reaction period in both oxic and anoxic systems and remained stable on the surface of the INP for 48 h.

The mechanisms of U-uptake were shown to be a coupled Fe–U redox reaction, as evidenced by the XPS analysis of nanoparticulate solids at various sampling period. The rapid reduction of U(VI) to U(IV) on the surfaces of the INP occurred concurrently with the oxidation of Fe(0) to Fe(II). Following a period of U-stability on the surfaces of the reacted INP in a reduced state (UO_{2+x}) the U was found to reoxidise and thus redissolve as the Fe(II) was reduced back to Fe(III).

This case study has demonstrated the potential application of INP as a low-cost remediation technology for complex U-contaminated solutions, be they from industrial or environmental origins.

Acknowledgements

We would like to thank Dr. Chung Choi from the Department of Earth Sciences, University of Bristol for performing the ICP-AES analysis. Research was funded by AWE plc under contract no. CDK0534/30002873 and we thank Mr Philip Purdie and Dr. Sean Amos at AWE for facilitating the project.

References

[1] W.-X. Zhang, C.-B. Wang, H.-L. Lien, Treatment of chlorinated organic contaminants with nanoscale bimetallic particles, Catal. Today 40 (1998) 387–395.
[2] P.G. Tratnyek, Putting corrosion to use: remediating contaminated groundwater with zero-valent metals, Chem. Ind-Lond. 13 (1996) 499–503.
[3] T. Bigg, S.J. Judd, Zero-valent iron for water treatment, Environ. Technol. 21 (2000) 661–670.
[4] R. Miehr, P.G. Tratnyek, J.Z. Bandstra, M.M. Scherer, M. Alowitz, E.J. Bylaska, Diversity of contaminant reduction reactions by zerovalent iron: role of the reductate, Environ. Sci. Technol. 38 (2004) 139–147.
[5] C.B. Wang, W.X. Zhang, Synthesizing nanoscale iron particles for rapid and complete dechlorination of TCE and PCBs, Environ. Sci. Technol. 31 (1997) 2154–2156.
[6] H.L. Lien, W.X. Zhang, Transformation of chlorinated methanes by nanoscale iron particles, J. Environ. Eng. 125 (1999) 1042–1047.
[7] H.L. Lien, W.X. Zhang, Nanoscale iron particles for complete reduction of chlorinated ethenes, Colloids Surf. A 191 (2001) 97–105.
[8] S. Choe, Y.Y. Chang, K. Y, J. Hwang, Khim, Kinetics of reductive denitrification by nanoscale zero-valent iron, Chemosphere 41 (2000) 1307–1311.
[9] R. Glazier, R. Venkatakrishnan, F. Gheorghiu, L. Walata, R. Nash, W.X. Zhang, Nanotechnology takes root, Civil Eng. 73 (2003) 64–69.
[10] S.M. Ponder, J.G. Darab, T.E. Mallouk, Remediation of Cr(VI) and Pb(II) aqueous solutions using supported, nanoscale zero-valent iron, Environ. Sci. Technol. 34 (2000) 2564–2569.
[11] B. Schrick, J.L. Blough, A.D. Jones, T.E. Mallouk, Hydrodechlorination of trichloroethylene to hydrocarbons using bimetallic nickel-iron nanoparticles, Chem. Mater. 14 (2002) 5140–5147.
[12] X.-Q. Li, W.-X. Zhang, Sequestration of metal cations with zerovalent iron nanoparticles: a study with high resolution X-ray photoelectron spectroscopy (HR-XPS), J. Phys. Chem. 111 (2007) 6939–6946.
[13] D.W. Elliott, W. Zhang, Field assessment of nanoscale biometallic particles for groundwater treatment, Environ. Sci. Technol. 35 (2001) 4922–4926.
[14] Y. Liu, S.A. Majetich, R.D. Tilton, D.S. Sholl, G.V. Lowry, TCE dechlorination rates, pathways, and efficiency of nanoscale iron particles with different properties, Environ. Sci. Technol. 39 (2005) 1338–1345.
[15] J.T. Nurmi, P.G. Tratnyek, V. Sarathy, D.R. Baer, J.E. Amonette, K. Pecher, C. Wang, J.C. Linehan, D.W. Matson, R.L. Penn, M.D. Driessen, Characterization and properties of metallic iron nanoparticles: spectroscopy, electrochemistry, and kinetics, Environ. Sci. Technol. 39 (2005) 1221–1230.
[16] R. Cheng, J.-L. Wang, W.-X. Zhang, Comparison of reductive dechlorination of p-chlorophenol using Fe-0 and nanosized Fe-0, J. Hazard. Mater. 144 (2007) 334–339.
[17] M.J. Alowitz, M.M. Scherer, Kinetics of nitrate, nitrite, and Cr(VI) reduction by iron metal, Environ. Sci. Technol. 36 (2002) 299–306.
[18] K. Mondal, G. Jegadeesan, S.B. Lalvani, Removal of selenate by Fe and NiFe nanosized particles, Ind. Eng. Chem. Res. 43 (2004) 4922–4934.
[19] J. Cao, D. Elliott, W.J. Zhang, Perchlorate reduction by nanoscale iron particles, J. Nanopart. Res. 7 (2005) 499–506.
[20] S.R. Kanel, B. Manning, L. Charlet, H. Choi, Removal of arsenic(III) from groundwater by nanoscale zero-valent iron, Environ. Sci. Technol. 39 (2005) 1291–1298.
[21] T. Shimotori, E.E. Nuxoll, E.L. Cussler, W.A. Arnold, A polymer membrane containing Fe-0 as a contaminant barrier, Environ. Sci. Technol. 38 (2004) 2264–2270.
[22] S.H. Joo, A.J. Feitz, D.L. Sedlak, T.D. Waite, Quantification of the oxidizing capacity of nanoparticulate zero-valent iron, Environ. Sci. Technol. 39 (2005) 1263–1268.
[23] A.J. Feitz, S.H. Joo, J. Guan, Q. Sun, D.L. Sedlak, T.D. Waite, Oxidative transformation of contaminants using colloidal zero-valent iron, Colloids Surf. A 265 (2005) 88–94.
[24] S.M. Ponder, J.G. Darab, J. Bucher, D. Caulder, I. Craig, L. Davis, N. Edelstein, W. Lukens, H. Nitsche, L.F. Rao, D.K. Shuh, T.E. Mallouk, Surface chemistry and electrochemistry of supported zerovalent iron nanoparticles in the remediation of aqueous metal contaminants, Chem. Mater. 13 (2001) 479–486.
[25] S.R. Kanel, J.M. Greneche, H. Choi, Arsenic(V) removal from groundwater using nano scale zero-valent iron as a colloidal reactive barrier material, Environ. Sci. Technol. 40 (2006) 2045–2050.
[26] D. Burghardt, E. Simon, K. Knöller, A. Kassahun, Immobilization of uranium and arsenic by injectible iron and hydrogen stimulated autotrophic sulphate reduction, J. Contam. Hydrol. 94 (2007) 305–314.
[27] O. Çelebi, Ç. Üzüm, T. Shahwan, H.N. Erten, A radiotracer study of the adsorption behavior of aqueous Ba^{2+} ions on nanoparticles of zero-valent iron, J. Hazard. Mater. 148 (2007) 761–767.
[28] J.G. Darab, A.B. Amonette, D.S.D. Burke, R.D. Orr., Removal of pertechnetate from simulated nuclear waste streams using supported zerovalent iron, Chem. Mater. 19 (2007) 5703–5713.
[29] T.B. Scott, Sorption of uranium onto iron bearing minerals, PhD Thesis, Interface Analysis Centre, University of Bristol, 2005.
[30] O. Riba, T.B. Scott, K.V. Ragnarsdottir, G.C. Allen, Reaction mechanism of uranyl in the presence of zero-valent iron nanoparticles, Geochim. Cosmochim. Acta 72 (2008) 4047–4057.
[31] C.D. Hsi, D. Langmuir, Adsorption of uranyl onto ferric oxyhydroxides. Application of the surface complexation site-binding model, Geochim. Cosmochim. Acta 49 (1985) 1931–1941.
[32] J.J. Lenhart, B.D. Honeyman, Uranium (VI) sorption to haematite in the presence of humic acid, Geochim. Cosmochim. Acta 63 (1999) 2891–2901.
[33] J.N. Fiedor, W.D. Bostick, R.J. Jarabek, J. Farrell, Understanding the mechanism of uranium removal from groundwater by zero-valent iron using x-ray photoelectron spectroscopy, Environ. Sci. Technol. 32 (1998) 1466–1473.
[34] J. Farrell, W.D. Bostick, R.J. Jarabek, J.N. Fiedor, Uranium removal from ground water using zero valet iron media, Ground Water 37 (1999) 618–624.
[35] K.J. Cantrell, D.I. Kaplan, T.W. Wietsma, Zero-valent iron for the in-situ remediation of selected metals in groundwater, J. Hazard. Mater. 42 (1995) 201–212.
[36] L. Charlet, E. Liger, P. Gerasimo, Decontamination of TCE- and U-rich waters by granular iron: role of sorbed Fe(II), J. Environ. Eng. 124 (1998) 25–30.
[37] E. Liger, L. Charlet, P. Van Cappellen, Surface catalysis of uranium(VI) reduction by iron(II), Geochim. Cosmochim. Acta 63 (1999) 2939–2955.
[38] S.J. Morrison, D.R. Metzler, C.E. Carpenter, Uranium precipitation in a permeable reactive barrier by progressive irreversible dissolution of zero-valent iron, Environ. Sci. Technol. 35 (2001) 385–390.
[39] B. Gu, L. Liang, M.J. Dickey, X. Yin, S. Dai, Reductive precipitation of uranium (VI) by zero-valent iron, Environ. Sci. Technol. 32 (1998) 3366–3373.
[40] R.M. Powell, R.W. Puls, S.K. Hightower, D.A. Sabatini, Coupled iron corrosion and chromate reduction: mechanisms for subsurface remediation, Environ. Sci. Technol. 29 (1995) 1913–1922.
[41] A.F. White, M.L. Peterson, Reduction of aqueous transition metal species on the surface of Fe(II)-containing oxides, Geochim. Cosmochim. Acta 60 (1996) 3799–3814.
[42] P. Wersin, M.F. Hochella Jr., P. Persson, G. Redden, J.O. Leckie, D.W. Harris, Interaction between aqueous uranium (VI) and sulphide minerals: spectroscopy evidence for sorption and reduction, Geochim. Cosmochim. Acta 58 (1994) 2829–2843.
[43] E.J. O'Loughlin, S.D. Kelly, R.E. Cook, R. Csencsits, K.M. Kemner, Reduction of uranium (VI) by mixed iron(II)/iron(III) hydroxide (green rust): formation of UO_2 nanoparticles, Environ. Sci. Technol. 37 (2003) 721–727.
[44] T. Missana, C. Maffiotte, M. García-Guttiérrez, Surface reaction kinetics between nanocrystalline magnetite and uranyl, J. Colloid Interface Sci. 261 (2003) 154–160.

[45] T.B. Scott, G.C. Allen, P.J. Heard, M.G. Randall, Reduction of U(VI) to U (IV) on the surface of magnetite, Geochim. Cosmochim. Acta 69 (2005) 5639–5646.
[46] AWE (private communications).
[47] Z.-W. Hao, X.-H. Xu, J. Jin, P. He, Y. Liu, D.-H. W., Simultaneous removal of nitrate and heavy metals by iron metal, J. Zhejiang Univ. SCI 6B (2005) 307–310.
[48] G.C.C. Yang, H.-L. Lee, Chemical reduction of nitrate by nano-sized iron. Kinetics and pathways, Water Res. 39 (2005) 884–894.
[49] Dayta Systems Ltd, c/o Interface Analysis Centre. http://daytasystems.co.uk.
[50] C. Noubactep, A. Schönerb, G. Meinrath, Mechanism of uranium removal from the aqueous solution by elemental iron, J. Hazard. Mater. 132 (2006) 202–212.
[51] L. Zhang, A. Manthiram, Chains composed of nanosize metal particles and identifying the factors driving their formation, Appl. Phys. Lett. 70 (1997) 2469–2471.
[52] T.B. Scott, M. Dickinson, R.A. Crane, O. Riba, G.M. Hughes, The effects of vacuum annealing on the structure and surface chemistry of iron nanoparticles. doi:10.1007/s11051-009-9767-y.
[53] N. Pernicone, F. Ferrero, I. Rossetti, L. Forni, P. Canton, P. Riello, G. Fagherazzi, M. Signoretto, F. Pinna, Wustite as a new precursor of industrial ammonia synthesis catalysts, Appl. Catal. A: Gen. 25l (2005) 121–129.
[54] G.C. Allen, M.T. Curtis, A.J. Hooper, M.J. Tucker, X-ray photoelectron spectroscopy of iron–oxygen systems, Chem. Soc. Dalton 14 (1974) 1525–1530.